A Preliminary Simulation of RF Power Evolution with Parametric Decay Processes during Lower Hybrid Wave Injection into Plasmas

Zikai Huang*, *Zhihao* Su, *Kunyu* Chen, *Long* Zeng, and *Zhe* Gao*

Department of Engineering Physics, Tsinghua University, Beijing, China

Abstract. Nonlinear interactions between radio frequency (RF) waves and plasmas have been researched for ages. We have developed a ray tracing program coupled with the nonlinear mechanism parametric decay instabilities (PDI) called Parametric Instabilities embedded Propagation and Evolution of RF Spectrum (PIPERS). The program can calculate the propagation and absorption in the scrape-off layer (SOL) plasma of lower hybrid waves (LHW) on the basis of the nonlocal convective amplification model of a quasi-mode PDI. To analyse the energy transfer and spectral evolution of LHW self-consistently and quantitatively, the characteristics of the numerical solution of the energy conservation equations need to be studied in terms of the simulation model.

1 Introduction

Radio frequency (RF) waves are important auxiliary ways for heating and current driving in magnetic confinement fusion devices [1]. As the power of RF waves and plasma parameters increase in present and future experiments, many nonlinear mechanisms during their interactions become significant, such as RF sheaths [2], ponderomotive force [3], beat wave excitation [4] and parametric decay instabilities (PDI) [5–7]. The improved nonlinear theories and quantitative simulations in detail are both required to get a more accurate and profound understanding of them.

Lower hybrid current drive (LHCD) was considered to be one of the most efficient methods for current driving in plasmas [8,9]. However, the spectral broadening and the nonlinear deposition of lower hybrid waves (LHW) at the plasma edge counters against its future application [10–13]. As a common nonlinear wave-wave interaction, PDI was supposed to be one of the main reasons in previous studies [10,14,15].

Recently, local and nonlocal models of LHW induced PDI have been promoted sufficiently [15–18]. The local models calculating the linear growth rates of different decay channels indicate that the PDI of LHW is a quasi-mode decay and the decay channels with large refractive indices parallel to the background magnetic field can't be ignored [15–17]. The nonlocal model [18] calculating the convective amplification factor as the saturation value of the quasi-mode decay allows us to implement a ray tracing program introduced PDI, which is called Parametric Instabilities embedded Propagation and Evolution of RF Spectrum (PIPERS). Given plasma parameters and wave parameters of certain device, PIPERS can calculate the propagation and absorption of LHW in the SOL plasma, preliminarily realizing a precise simulation of PDI.

In the present paper, we mainly demonstrate the characteristics of the numerical solutions of PIPERS. The basic physical equations and simulation model are encapsulated for completeness in Section 2, which will be detailed in other articles. In Section 3, the numerical solutions of the basic equations are displayed. The discussion and conclusions are introduced in Section 4.

2 Basic equations and model

PDI is a common nonlinear wave-wave interaction in plasmas, which excitation conditions are,

$$\begin{cases}\omega_1 = \omega_{\mathrm{LF}} - \omega_0 \\ \boldsymbol{k_1} = \boldsymbol{k_{LF}} - \boldsymbol{k_0}\end{cases}. \tag{1}$$

where ω and $\boldsymbol{k}$ are the frequency and wave vector of the waves, the subscripts 0, 1, LF represent the pump wave, the lower sideband wave and the low frequency wave ($\omega_{\mathrm{LF}} << \omega_{0,1}$) respectively.

For a quasi-mode decay of PDI, the low frequency wave is a quasi-mode [15,19], deviating from the linear dispersion relation severely; while the other two waves satisfy the linear dispersion relation. Thus, there are abundant decay channels given by a simple sum of the wave vectors $\boldsymbol{k}_{\mathrm{LF}} = \boldsymbol{k_0} + \boldsymbol{k_1}$ in wave parameter space $\{\omega_1, \boldsymbol{k_1}\}$. And the pump energy is mainly transferred to the lower sideband waves when PDI occurs [6,20], according to the matching conditions eq. (1). Hence, the propagation and energy evolution of the two high frequency waves are crucial for calculation of PDI, which can be described by the WKB theory [21].

Firstly, the ray tracing equations of the pump wave and the sideband waves are,

*Corresponding authors: huangzk23@mails.tsinghua.edu.cn
gaozhe@tsinghua.edu.cn

$$\begin{cases} \dot{\boldsymbol{r}}_{\boldsymbol{j}} = -\frac{\partial D_j/\partial k_j}{\partial D_j/\partial \omega_j} = \frac{\partial \omega_j}{\partial k_j} = v_{jg} \\ \dot{\boldsymbol{k}}_{\boldsymbol{j}} = \frac{\partial D_j/\partial r_j}{\partial D_j/\partial \omega_j} = -\frac{\partial \omega_j}{\partial r_j} \end{cases} . \quad (2)$$

where $D_j(\omega_j, \boldsymbol{k_j}, \boldsymbol{r_j}) = 0$ is the linear dispersion relation, $\boldsymbol{v_{jg}}$ is the group velocity, $\boldsymbol{r_j}$ is the position of the high frequency waves $j = 0,1$.

Considering the weak damping of the pump wave at the cold edge, it is ignored along with the energy of the low frequency wave. Due to the constraint of the lower sideband waves by the convective amplification process of PDI [22], the spatial energy conservation equations of PDI can be expressed as

$$\begin{cases} \nabla \cdot \boldsymbol{P_0} + \int_{\omega_1, k_1} (\nabla \cdot \boldsymbol{P_1} - 2\gamma_{1L} U_1) = 0 \\ U_1 = U_{\text{th}} \exp[2A] \end{cases} . \quad (3)$$

where $\boldsymbol{P_0}$ is the power flux of the pump wave, the integration in the wave parameter space represents the calculation of all the decay channels. $\boldsymbol{P_1} = U_1 \boldsymbol{v_{1g}}$ is the power flux, γ_{1L} is the linear damping rate, and U_1 is the energy density of a certain sideband wave. U_{th} is the initial value and A is the convective amplification factor, representing the convective amplification process of PDI [18]. As they are deeply coupled with each other and hard to solve, some simplifications for numerical solving in simulation has been adopted.

Because PDI can be suppressed by high plasma temperature [15,17], the simulation region is located at the cold edge. Its radial size is much smaller than the toroidal and poloidal size. Therefore, RF waves are considered to propagate in a slab plasma in Cartesian coordinates, where x, y, z represent the radial, poloidal and toroidal directions respectively. The plasma parameters are assumed to vary along the x-axis only and the background magnetic field is set to z-axis.

Due to the nonzero parallel refractive index, the pump wave slightly deviates towards the z-axis when propagating into the plasma along the x-axis. And there is a pump region, which cross section of y-z plane is equal to the antenna and power density depends on x-axis only. The abundant sideband waves in the wave parameter space can propagate from any position in the pump region variously, but only the parts remained in the pump region of their trajectories can be amplified.

Considering volume integration and Divergence Theorem, we can slice the pump region along the x-axis to iteratively solve eq. (3) in the simulation region. The forward differential form of the power flux equations between the pump slices are,

$$\begin{cases} P_{0x}(x_{n+1}) = P_{0x}(x_n) - \sum_s \left(P_s(x_{n+1}) - D_s(x_{n+1})\right) \\ P_s(x_{n+1}) = U_{\text{sth}} \, exp\left(2A_s(x_{n+1})\right) \cdot F_s(x_{n+1}) \\ D_s(x_{n+1}) = \sum_l 2\gamma_{sL}(x_l) U_{\text{sth}} \, exp\left(2A_s(x_l)\right) \cdot F_s(x_l) \end{cases} . \quad (4)$$

where subscript s refers to different decay channels, subscript x refers to the component in the x-direction. $P_{0x}(x_n)$ and $P_{0x}(x_{n+1})$ are the power flux of the pump wave flowing in and outs the slice. $P_s(x_{n+1})$ and $D_s(x_{n+1})$ are the power flux of the sideband waves flowing out the slice and the dissipation along their trajectories. The summation of l represent the trajectory remained in the pump region until this slice. U_{sth} and A_s are the initial power density and the convective amplification factor. F_s is the modulus of the converted energy flow vector in the slice. $\Delta x = x_{n+1} - x_n$ is the width of the slices, which is usually expected to be much smaller than the spatial scale of the plasma parameter variation.

When the pump energy is transferred to a certain decay channel, the initial value depends on the wave parameters and the volume occupied in the wave parameter space; while the convective amplification factor and dissipation depend on the wave parameters and the trajectory remained in the pump region. Additionally, the energy transfer is a competitive process for different decay channels due to the pump depletion. Thus, the sampling of the sideband waves included needs to be dense and wide coverage in the wave parameter space.

Based on the aforementioned discussions, the width of the pump slices and the sampling of the sideband waves play important roles in the accuracy of the numerical solution of eq. (4). However, small width of the pump slices causes many calculation steps and many sideband waves lead to heavy load on memory, which both consume a lot of computation time. In order to save computing resources as much as possible while ensuring the accuracy and convergence of the numerical solutions, we have conducted many simulation tests to select appropriate sampling and slicing parameters, which will be illustrated in the next section.

3 Simulation Results

3.1 Input parameters

The basic input parameters of PIPERS for the simulation tests are chosen as the typical plasma parameters and wave parameters of JET [10], where there is almost no significant PDI.

The background magnetic field is $B_T = 3.4$ T at the major radius $R = 2.96$ m. The profiles of the plasma density and temperature from the antenna around the SOL are shown in Fig. 1. The LHW antenna is located at the origin, where $n_e \sim 3 \times 10^{17} \text{m}^{-3}$ and $T_e \sim 8$ eV. The last closed flux surface (LCFS) is located around $x = 0.05$ m, where $n_e \sim 1 \times 10^{19}$ m^{-3} and $T_e \sim 2\,0$ eV. The LHW frequency is $f_0 = 3.7$ GHz and its parallel refractive index is $N_{0z} = 1.84$. The major radius coordinates of the LHW antenna is $R_{\text{antenna}} = 3.89$ m. The poloidal and toroidal lengths of the antenna mouth are $L_y = 0.884$ m and $L_z = 0.348$ m. And the power injected is chosen as $P_0 = 2$ MW.

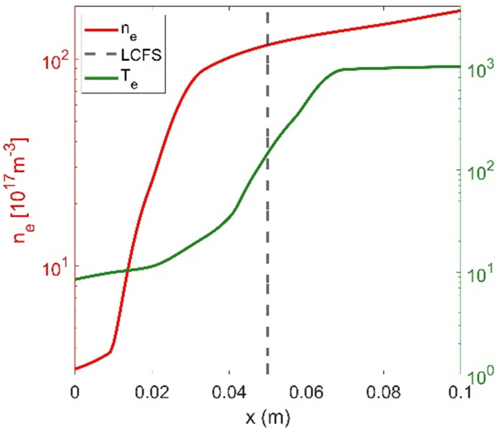

Fig. 1. The profiles of the plasma density and temperature from the antenna around the SOL of JET used for simulation on PIPERS. The red curve refers to the plasma density and the green curve refers to the plasma temperature. The antenna is located at the origin and the LCFS is located at $x = 0.05$ m.

3.2 Characteristics of the sampling

Due to the linear dispersion relation and the PDI excitation conditions [15,17], the wave parameter space $\{\omega_1, \boldsymbol{k_1}\}$ can be reduced to the three dimensions $\{\omega_{\mathrm{LF}}, \theta_1, N_{1z}\}$. ω_{LF} is the frequency of the low frequency wave, ranging from ion sound frequency to several ion cyclotron frequency ω_{ci} · θ_1 is the scattering angle, defined as the angle between the components perpendicular to the background magnetic field of the wave vector $\boldsymbol{k_0}$ and $\boldsymbol{k_1}$. $N_{1z} = ck_{1z}/\omega_0$ is the refractive index parallel to the background magnetic field of the sideband wave defined with the pump frequency ω_0.

Actually, the decay channels with excessive parallel refractive index or multiple harmonic ion cyclotron frequency are hard to grow due to strong Landau damping and small coupling coefficients. According to the geometric relation of the new wave parameters [17], the sideband waves will propagate in the opposite x-direction when $|\theta_1| > 90°$, where there is no plasma. And the sideband waves can't propagate into the pump region when $|N_{1z}| < 2$ due to the accessibility. Above all, the sampling range are selected as $\omega_{\mathrm{LF}} \in \{0{,}20\omega_{\mathrm{ci}}\}$, $\theta_1 \in \{-90°, 90°\}$ and $N_{1z} \in \{-80, -2\} \cup \{2{,}80\}$, basically covering all the decay channels with positive linear growth rates.

Given the input parameters and number of sampling points within the sampling ranges, PIPERS can solve the energy evolution equations and calculate the portion of energy transfer. It's noted that the plasma density has been increased by 30% and the plasma temperature has been decreased by 20% based on the input parameters in Section 3.1 in order to enhance the PDI intensity to obtain better comparative effect. The portion of the rest pump power tends to be constant when the number of sampling points of one dimension is gradually increased and other two dimension remain unchanged, as is shown in Fig. 2-4.

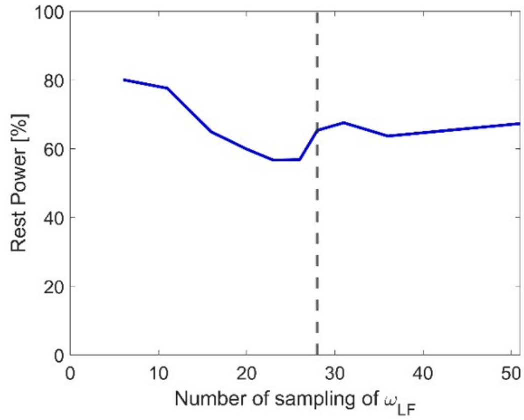

Fig. 2. The portion of the rest pump power as the number of sampling points of the frequency increases. The dashed line corresponds to $\Delta\omega_{\mathrm{LF}} \approx 0.2\omega_{\mathrm{ci}}$. The sampling interval of other dimensions are kept $\Delta\theta_1 = 1°$ and $\Delta N_{1z} = 2$. The input parameters are as mentioned above.

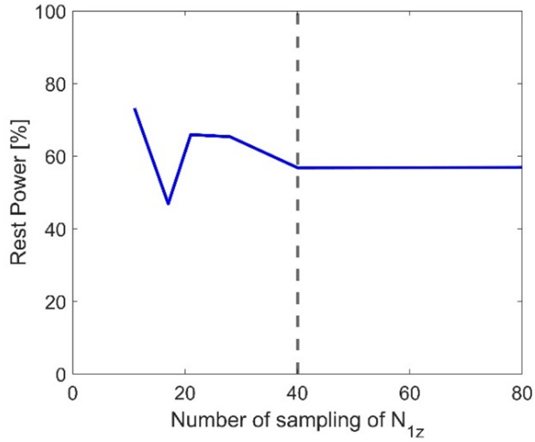

Fig. 3. The portion of the rest pump power as the number of sampling points of the parallel refractive index increases. The dashed line corresponds to $\Delta N_{1z} = 2$. The sampling interval of other dimensions are kept $\Delta\theta_1 = 1°$ and $\Delta\omega_{\mathrm{LF}} = 0.2\omega_{\mathrm{ci}}$. The input parameters are the same as Fig. 2.

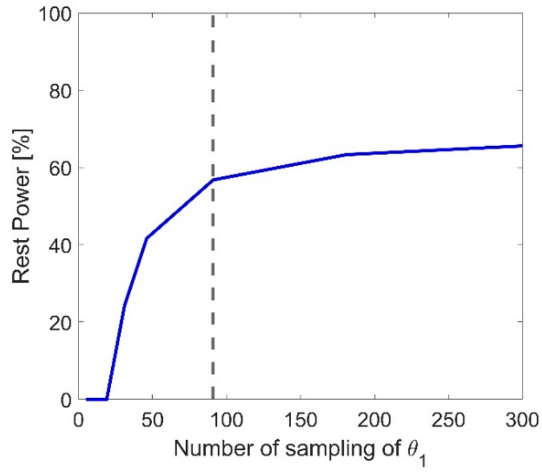

Fig. 4. The portion of the rest pump power as the number of sampling points of the scattering angle increases. The dashed line corresponds to $\Delta\theta_1 = 1°$. The sampling interval of other dimensions are kept $\Delta\omega_{\mathrm{LF}} = 0.2\omega_{\mathrm{ci}}$ and $\Delta N_{1z} = 2$. The input parameters are the same as Fig. 2.

According to the simulation results shown in Fig. 2-4, the portion of the rest pump power is more sensitive to the number of sampling points of the scattering angle than the other two dimensions. That's because the distribution of the decay channels with large convective amplification factors in scattering angle space is more peaked, leading to denser sampling. Besides, sampling in frequency and parallel refractive index space requires a certain degree of density to ensure spectral precision, although it can be taken sparser when the calculation is only for the portion of energy transfer. To balance the memory load and the accuracy of the results, $\Delta\omega_{\mathrm{LF}} = 0.2\omega_{\mathrm{ci}}$, $\Delta\theta_1 = 1^\circ$, $\Delta N_{1z} = 2$ (dashed lines in Fig. 2-4) are chosen to be the appropriate intervals to sampling the decay channels.

3.3 Characteristics of the pump slicing

As is mentioned before, the width of the pump slices Δx should be much smaller than the spatial scale of the plasma parameter variation, leading to a large number of slices and long computation time. It's noted that the plasma density has been increased by 10% based on the input parameters in Section 3.1 in order to enhance the PDI intensity to obtain better comparative effect. Given the slices' width, the variation of the portion of the rest pump power is shown in Fig. 5.

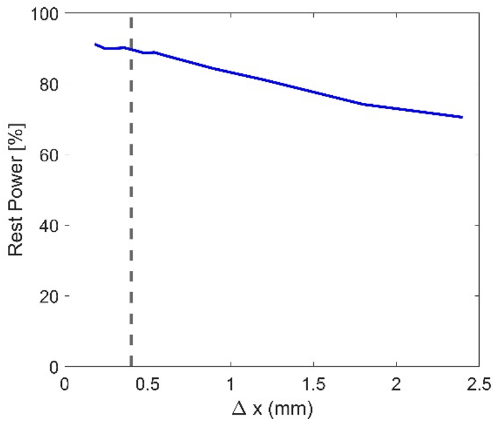

Fig. 5. The portion of the rest pump power as the width of the pump slices changes from 0.18 mm to 2.4 mm. The sampling intervals adopted are verified in Section 3.2 and the input parameters are as mentioned above.

With the width of the pump slices shortening, the portion of the rest pump power is calculated more precisely but the calculation is much more time-consuming. To balance the computation time and the accuracy of the results, the width of the pump slices is chosen as $\Delta x = 0.4$ mm (dashed line in Fig. 5), generating hundreds of slices within a few centimeters around the SOL.

3.4 Characteristics of the frequency spectrum

After the characteristic investigation of the sideband wave sampling and the pump slicing, the simulation results can reproduce some experimental observations credibly. Except the portion of the energy transfer, PIPERS can also illustrate the frequency spectral evolution throughout the entire propagation process with the recorded information of the sampled sideband waves, as is shown in **Fig. 6** and [23].

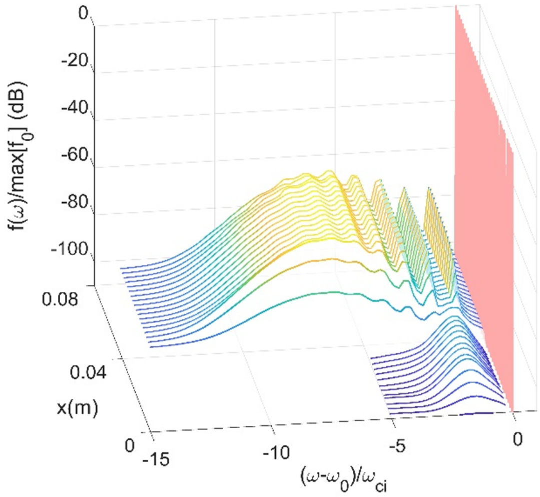

Fig. 6. The evolution of the frequency spectrum as the pump propagation depth increases. The steep and high peak at the right side refers to the pump power. The other short peaks are the sideband waves. $(\omega - \omega_0)/\omega_{\mathrm{ci}}$ represents the position on the frequency spectrum normalized by ω_{ci}. $f(\omega)/\,max[f_0]$ is the power density compared to the initial pump wave in decibels. x is the depth of propagation. The input parameters are shown in Section 3.1.

The propagation process is divided into two areas, which are calculated separately. One is near the antenna, dominated by the ion sound quasi-mode. The other is near the LCFS, dominated by the ion cyclotron quasi-mode. [17] Clearly, the decay channels with high harmonics ion cyclotron frequency merge and obtain more energy than those with one or two harmonics ion cyclotron frequency. The wave parameters, plasma parameters, the sampling and slicing methods can determine the relative and absolute intensity of the spectrum. Only the wave and plasma parameters affect the shape and position of the sideband peaks. The sampling and slicing methods affect the spectral resolution. Although there is almost no energy loss of the pump wave in condition of the input parameters in Section 3.1, there are still spectral broadening beyond experimental observation as the LHW propagates into the plasma.

4 Discussion and conclusions

Based on the improved local and nonlocal PDI models [17,18], we have developed the program PIPERS to calculate the propagation and energy transfer in the SOL plasma in condition of the quasi-mode decay PDI of LHW.

Due to the complexity arising from the deeply coupling of the energy evolution equations, the characteristics of their numerical solution require careful investigation to ensure the accuracy and convergence of the simulation results. With typical parameters in experiments of JET, some preliminary simulation tests have been designed to confirm the characteristics of the sampling in the wave parameter space and the iterative calculating between the pump slices while saving the computation time as much as possible. After that, PIPERS can not only calculate the portion of the rest pump power but also the spectral evolution of PDI, being able to conclude the PDI intensity and main decay channels in certain experimental or virtual scenarios.

Consequently, PDI is an important nonlinear mechanism of wave-wave interaction in fusion plasmas. Quantitative simulation with a verified program based on improved models is also an important method to study related experimental phenomena in detail. Experiments of more devices will be simulated on PIPERS with further optimization in the future.

This work was supported by NSFC, under Grant No. 12335014.

References

[1] J. Wesson and D. J. Campbell, Tokamaks, 4th ed, (Oxford University Press, Oxford, New York, 2011).

[2] Y. Li et al., Characterization of SOL profiles and turbulence in ICRF-heated plasmas in EAST, Nucl. Fusion **64**, 056023 (2024). https://doi.org/10.1088/1741-4326/ad3564

[3] Z. Gao, N. J. Fisch, and H. Qin, Nonlinear ponderomotive force by low frequency waves and nonresonant current drive, Physics of Plasmas **13**, 112307 (2006). https://doi.org/10.1063/1.2397584

[4] M. N. Rosenbluth and C. S. Liu, Excitation of Plasma Waves by Two Laser Beams, Phys. Rev. Lett. **29**, 701 (1972). https://doi.org/10.1103/PhysRevLett.29.701

[5] M. N. Rosenbluth, Parametric Instabilities in Inhomogeneous Media, Phys. Rev. Lett. **29**, 565 (1972). https://doi.org/10.1103/PhysRevLett.29.565

[6] Y. Takase and M. Porkolab, Parametric excitation of ion-sound quasimodes during lower-hybrid heating experiments in tokamaks, The Physics of Fluids **26**, 2992 (1983). https://doi.org/10.1063/1.864022

[7] C. S. Liu and V. K. Tripathi, Parametric Instabilities in a Magnetized Plasma, Physics Reports **130**, 143 (1986). https://doi.org/10.1016/0370-1573(86)90108-0

[8] N. J. Fisch, Theory of current drive in plasmas, Rev. Mod. Phys. **59**, 175 (1987). https://doi.org/10.1103/RevModPhys.59.175

[9] J. Freidberg, Plasma Physics and Fusion Energy, (Cambridge University Press, 2007).

[10] R. Cesario, A. Cardinali, C. Castaldo, F. Paoletti, W. Fundamenski, S. Hacquin, and T. J.-E. W. Contributors, Spectral broadening of lower hybrid waves produced by parametric instability in current drive experiments of tokamak plasmas, Nucl. Fusion **46**, 462 (2006). https://doi.org/10.1088/0029-5515/46/4/007

[11] S. G. Baek, R. R. Parker, P. T. Bonoli, S. Shiraiwa, G. M. Wallace, B. LaBombard, I. C. Faust, M. Porkolab, and D. G. Whyte, High density LHRF experiments in Alcator C-Mod and implications for reactor scale devices, Nucl. Fusion **55**, 043009 (2015). https://doi.org/10.1088/0029-5515/55/4/043009

[12] M. H. Li et al., Observation and analysis of lower-hybrid-current-drive density limit in EAST, Nucl. Fusion **62**, 126055 (2022). https://doi.org/10.1088/1741-4326/ac99ed

[13] S. Ide, O. Naito, T. Kondoh, Y. Ikeda, and K. Ushigusa, Enhancement of Absorption of Lower Hybrid Wave by Filling the Spectral Gap, Phys. Rev. Lett. **73**, 2312 (1994). https://doi.org/10.1103/PhysRevLett.73.2312

[14] M. Porkolab, Theory of parametric instability near the lower-hybrid frequency, The Physics of Fluids **17**, 1432 (1974). https://doi.org/10.1063/1.1694910

[15] A. Zhao and Z. Gao, Parameter study of parametric instabilities during lower hybrid wave injection into tokamaks, Nucl. Fusion **53**, 083015 (2013). https://doi.org/10.1088/0029-5515/53/8/083015

[16] Z. Liu, Z. Gao, and A. Zhao, Kinetic theory of parametric instabilities of lower hybrid waves in tokamaks in the electromagnetic framework, Physics of Plasmas **27**, 042503 (2020). https://doi.org/10.1063/1.5139281

[17] Z. Gao, Z. H. Su, Z. R. Liu, Z. K. Huang, J. Y. Han, and Z. Y. Liu, Kinetic theory of parametric instabilities in magnetized plasmas and its application to analyzing decay waves during the injection of lower hybrid waves, Nucl. Fusion **65**, 046033 (2025). https://doi.org/10.1088/1741-4326/adbcc4

[18] K. Chen and Z. Gao, Saturation of a quasi-mode parametric instability in an inhomogeneous plasma, Nucl. Fusion **65**, 036020 (2025). https://doi.org/10.1088/1741-4326/adb0de

[19] Z. Liu, Z. Gao, and A. Zhao, Nonlinearity in parametric instabilities during the injection of lower hybrid waves into tokamak plasmas, Physics of Plasmas **26**, 042117 (2019). https://doi.org/10.1063/1.5088553

[20] L. Chen and R. L. Berger, Spatial depletion of the lower hybrid cone through parametric decay, Nucl. Fusion **17**, 779 (1977). https://doi.org/10.1088/0029-5515/17/4/011

[21] D. G. Swanson, Plasma Waves, 2nd ed., (Institute of Physics Pub, Bristol, Philadelphia, 2003).

[22] Kunyu Chen, Zhihao Su, Zikai Huang, Long Zeng and Zhe Gao, Theoretical Scaling of the Nonlinear Density Limit of Lower Hybrid Current Drive, 25th Topical Conference on Radio-Frequency Power in Plasmas, Schloss Hohenkammer, Germany, 19-22 May (2025).

[23] Zhe Gao, Kunyu Chen, Zhihao Su, Zikai Huang, and Long Zeng, Spectrum Evolution and Density Limit in Self-Consistent Modeling of Lower Hybrid Wave Propagation with Parametric Instabilities, 25th Topical Conference on Radio-Frequency Power in Plasmas, Schloss Hohenkammer, Germany, 19-22 May (2025). https://www.ipp.mpg.de/5533925